Available online at www.sciencedirect.com
ScienceDirect
PHOTONICS AND NANOSTRUCTURES Fundamentals and Applications
Photonics and Nanostructures – Fundamentals and Applications xxx (2015) xxx–xxx
www.elsevier.com/locate/photonics

Multi-directional ultra-high sensitive pressure sensor based on the integration of optimized double 60° bend waveguides and modified center-defect photonic crystal microcavity

Jian Zhou, Daquan Yang, Huiping Tian *, Lijun Huang, Pan Zhang, Yuefeng Ji

The State Key Laboratory of Information Photonics and Optical Communications, School of Information and Communication Engineering, Beijing University of Posts and Telecommunications, Beijing 100876, China

Received 30 September 2014; accepted 9 January 2015

Abstract

In the previous work [1], we have proposed a method to realize multi-directional pressure sensor. This follow-up work provides an optimized structure design based on the integration of double 60° bend waveguides and modified center-defect photonic crystal microcavity to further improve sensitivity. By applying two-dimensional finite difference time domain technologies (2D-FDTD) and finite-element methods (FEM), we systematically investigate the variations of optical properties under applied pressure. Linear relationships between the resonant wavelength shift and the applied pressure are obtained in three directions. The ultra-high sensitivities and the low minimum detectable pressure in longitudinal, transverse and upright directions are 39.7 nm/μN and 1.08 nN, 30.20 nm/μN and 1.43 nN, and 0.12 nm/nN and 0.36 nN respectively.

Keywords: Photonic crystals; Optical sensing and sensors; Optical resonators; Multi-directional pressure sensor

1. Introduction

Since the first demonstration [2], photonic crystal (PhC) nanocavities have attracted much interest and shown the abilities of strongly controlling photons in a wavelength-scale resonator with very low loss [3,4]. During the past decades, PhC nanocavities with energy concentration in one- or half-wavelength cubic volume have been very beneficial for enhancing interactions between light and matters in quantum-electro-dynamic phenomenon studies [5], opto-mechanical researches [6,7], and optical sensing applications [8–15]. Recently, attributing to the rapid development of nano/micro-fabrication technologies, the optical micro-electromechanical systems (MEMS) are widely developed for various optical sensors in micro-chip scale with fine or even higher sensitivity than that conventional ones. PhC sensors, due to the attractive characteristics such as compact size, high sensitivity, accurate limit of detection and easier integration, have been a candidate to realize further minimization and high performance of the system.

In addition, mechanical sensing effects of PhC structures have also been reported so far [16–25]. Xu et al. [16] demonstrated a micro displacement sensor based

* Corresponding author at: Beijing University of Posts and Telecommunications, P.O. Box 90, #10 Xitucheng Road, Haidian District, Beijing 100876, China. Tel.: +86 10 62282153.
E-mail address: hptian@bupt.edu.cn (H. Tian).

http://dx.doi.org/10.1016/j.photonics.2015.01.005
1569-4410/

Please cite this article in press as: J. Zhou, et al. Multi-directional ultra-high sensitive pressure sensor based on the integration of optimized double 60° bend waveguides and modified center-defect photonic crystal microcavity, Photon Nanostruct: Fundam Appl (2015), http://dx.doi.org/10.1016/j.photonics.2015.01.005

on PhC line-defect resonant cavity structure by monitoring the intensity of transmission spectra as a token of the displacement. Lee et al. [18,19] proposed stress sensors with high sensitivity based on PhC which measured changes in the resonant frequency in transmission spectra when forces were applied on the cantilever. Yang et al. [20] demonstrated PhC stress sensor with high sensitivity in double directions based on shoulder-coupled aslant nanocavity. Lu and Lee [22] proposed the stress sensor utilized double-layered photonic crystal cavity. Tung et al. [23] investigated the strain sensing effect in modified single-defect photonic crystal nanocavity. In addition, Yang et al. [25] presented the torsion-free photonic crystal pressure sensor with ultra-high sensitivity based on side-coupled piston-type microcavity. However, in these studies, the generated stress on these measurements was just taken along in one or two directions.

In this paper, we demonstrate a pressure sensor with ultra-high sensitivity based on the integration of double ultra-low-loss 60° bend waveguides and high quality factor modified center-defect photonic crystal microcavity in three directions (x–y–z (transverse–longitudinal–upright)). The architecture consists of a modified center-defect microcavity coupled to two symmetrical W1 waveguides, which combines unique advantages of double optimized photonic crystal 60° bend waveguides and modified center-defect microcavity. In this configuration, the resonant cavity is placed between two terminated Γ–K waveguides that are displaced along the Γ–M direction. The whole structure is symmetric with respect to its center to obtain a stronger coupling strength. The cavity is shoulder-coupled [26] to leak the light inside the cavity onto the output waveguide for detecting the resonance wavelength in transmittance spectra. With this pressure sensor fixed on the base, the pressure is measured by the resonance wavelength shift, which is caused through the mechanical deformation of microcavity resonator. The linear relationship between the applied pressure and corresponding structural variation is calculated and analyzed by finite-element method (FEM). The basic model properties and optical spectra response for structural variations will be investigated by finite difference time domain (FDTD) simulations. The theoretically calculated sensitivities of 39.70 nm/μN in longitudinal direction, 30.20 nm/μN in transverse direction and 0.12 nm/nN in upright direction are obtained. The minimum detectable pressure is approximately of 1.08 nN, 1.43 nN, and 0.36 nN in longitudinal, transverse and upright directions for this model, respectively.

2. PhC structure design

In this paper, Yang et al. [30] have demonstrated the fundamental schematic of the modified center-defect photonic crystal microcavity and the directions of physical variation applied, which consists of two sections. One section is a movable substrate which is located below the whole device. PhC structure as a pressure sensing element is placed on the substrate, the center of the PhC structure is fixed and the other side boundaries are free in order to generate deformation when the boundaries are under applied pressure. Pressure generated by applying stress to the free-boundary of PhC structure will be parallel to the light propagation direction, so-called transverse pressure, and the pressure that is perpendicular to the light propagation direction is called longitudinal pressure. The designed structure is the triangular lattice silicon (Si, $n_{si} = 3.4$) which is composed of PhC microcavity shoulder-coupled between two W1 waveguide and the PhC structure centro-symmetric as shown in Fig. 1. Here PhC microcavity is achieved by adding a nanohole in the center of the H_2-cavity [31]. Additionally, the three outer holes on the two sides of the defect are modified to improve in-plane confinement of light, while the other holes remain constant. The radius of air holes is 136 nm ($r = 0.32a$) and the lattice constant is $a = 425$ nm. The other section consists of the Si-strip trestle and an inserted rod located on the PhC microcavity. Meanwhile, we also believe that this proposed pressure sensor structure can benefit our efforts toward realizing fully valuable photonics and sensor societies. In this paper, light source is placed at the head of input waveguide and monitor is placed at the end of output waveguide. Additionally, a preliminary analysis of the structure has been performed by using the open source FDTD software Meep [34,35] to calculate the transmission spectra and field profile.

As shown in Fig. 1(b), the PhC microcavity is shoulder-coupled between two W1 waveguides and PhC structure is centro-symmetric in top view. Air holes in the W1 waveguide are removed until the hole along the direction (60° aslant direction) of PhC microcavity to achieve the best coupling strength. The transmission can be very high because the light-wave experiences the least difference between propagating along the straight waveguide and through the bend waveguide [36–40]. As a result, in order to minimize the loss caused by the mode patterns mismatch between the guided modes in the straight waveguide (Γ–K direction) and the waveguide bend (Γ–M direction), we move the air holes (blue holes at the corner of the bend) oppositely along the symmetric axis of the bend and change these holes radius to optimize the bend performance. The air holes have

Please cite this article in press as: J. Zhou, et al. Multi-directional ultra-high sensitive pressure sensor based on the integration of optimized double 60° bend waveguides and modified center-defect photonic crystal microcavity, Photon Nanostruct: Fundam Appl (2015), http://dx.doi.org/10.1016/j.photonics.2015.01.005

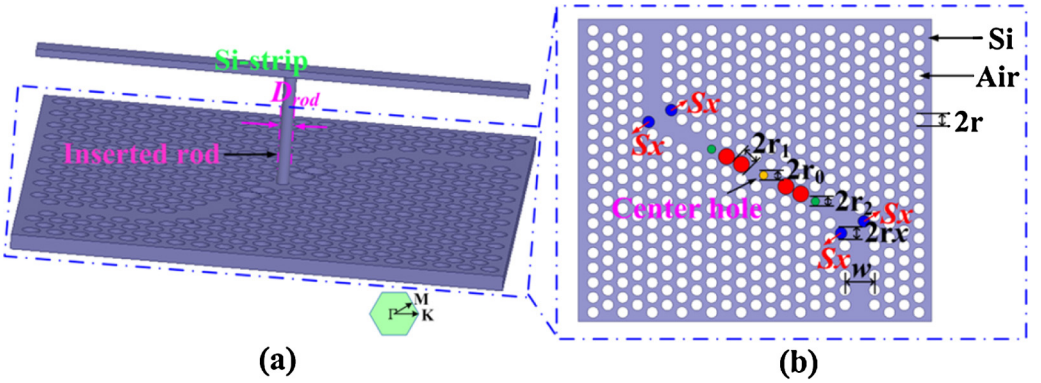

Fig. 1. (a) The schematic diagram of modified center-defect PhC microcavity and optimized double 60° bend waveguides design; (b) the detailed parameters of the PhC structure. Here lattice shift $Sx = 0.32a$, air-hole radius $rx = 0.32a$, $r_1 = 0.38a$, $r_2 = 0.19a$. (For interpretation of the references to color in text, the reader is referred to the web version of this article.)

the radii of $rx = 0.32a$, and they are moved by $0.32a$ ($Sx = 0.32a$) oppositely along the symmetric axis of the bend (the Γ–M direction). Then, a nanohole is added in the center of H_2-cavity of the proposed PhC microcavity. Here, the air-hole radius r_1 and r_2 are set to be $0.38a$, and $0.19a$, respectively. The radius of the modified center-defect nanohole is r_0. We use Meep to design and optimize the cavity about the dependence of the central nanohole (r_0) so that two main optical characteristics are taken to be considered: resonant frequency and quality factor. The radius of nanohole r_0 varies from 0 to $0.22a$ with an increment of $0.02a$. Fig. 2 shows the variation tendency of the resonant frequency and quality factor in terms of the central nanohole radius r_0. From Fig. 2, we observe the resonant frequency is pushed toward to higher frequencies when the central nanohole radius increases. This is because the larger central nanohole radius provides more low-dielectric region inside the cavity. When $r_0 = 0.15a$ and the resonant frequency $\omega = 0.2766$ ($2\pi c/a$), the highest quality factor $Q = 3.6 \times 10^4$ is obtained because the maximum mode field overlap is realized in this structure. Therefore, we employ this optimized model to realize high-sensitivity sensor. Fig. 3 shows the calculated output transmission spectrum of TE-like polarized light-wave when the geometric parameters of Sx, rx, r_1, r_2 and r_0 are adjusted to $0.32a$, $0.32a$, $0.38a$, $0.19a$ and $0.15a$, respectively.

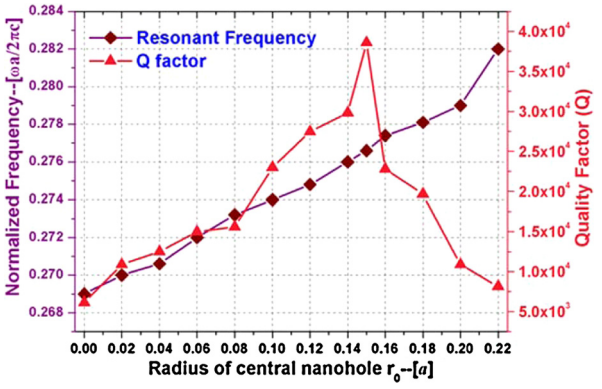

Fig. 2. Results of FDTD calculations showing resonant frequencies and quality factors as function of central nanohole radius r_0 ranging from $r_0 = 0$ to $r_0 = 0.22a$.

3. FEM simulated structural variation

3.1. Structural variation in longitudinal and transverse directions

First, changes in the geometry of the PhC when subject to pressure are analyzed using commercial FEM software ANSYS^{TM} 13.0. Then, these variations in

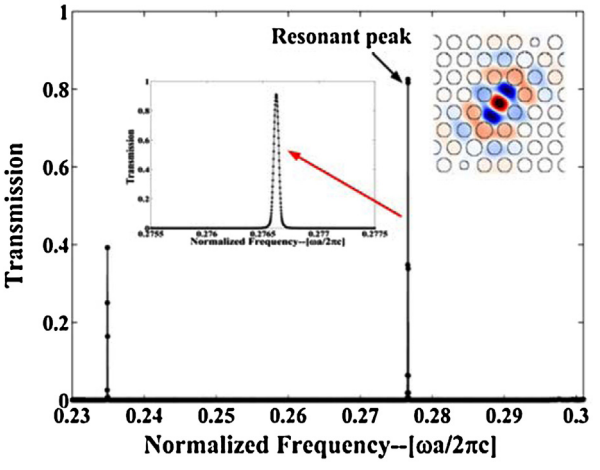

Fig. 3. FDTD spectrum, the inset shows the amplified image of the resonant peak and intensity profile of a simulation showing the corresponding output transmission degenerate mode, respectively.

Please cite this article in press as: J. Zhou, et al. Multi-directional ultra-high sensitive pressure sensor based on the integration of optimized double 60° bend waveguides and modified center-defect photonic crystal microcavity, Photon Nanostruct: Fundam Appl (2015), http://dx.doi.org/10.1016/j.photonics.2015.01.005

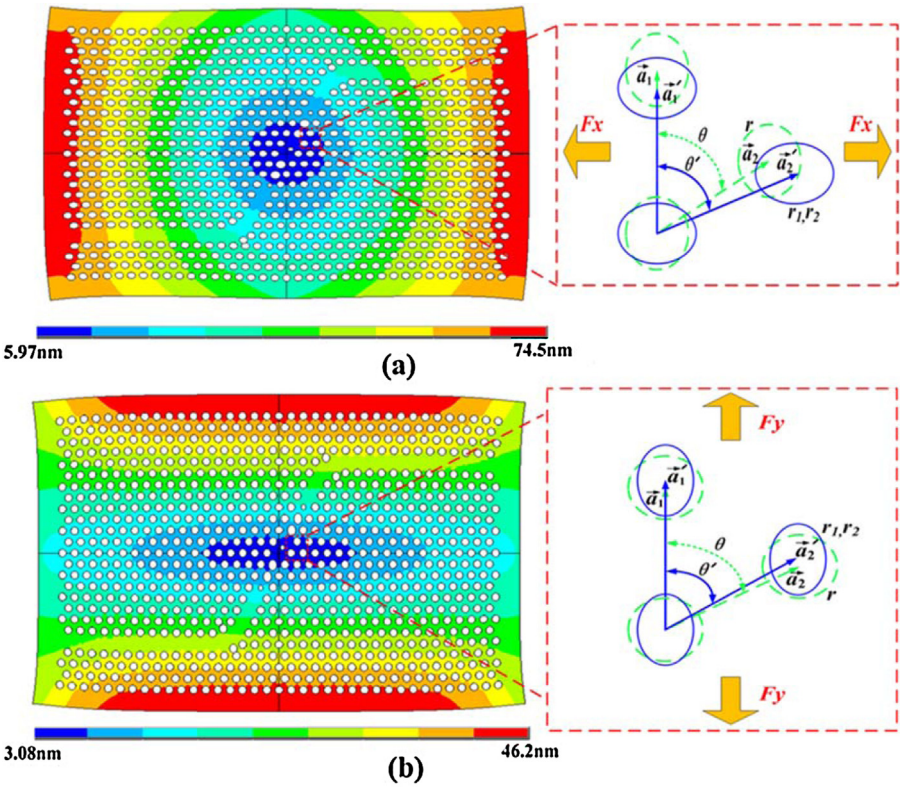

Fig. 4. Deformation of PhC structure under applied pressure using FEM simulation in (a) transverse direction and (b) longitudinal direction. Deformation contour plot of the model under −0.4 μN pressure load, the red dashed framed parts show that the initial and under-pressure shapes of PhC structure.(For interpretation of the references to color in this figure legend, the reader is referred to the web version of this article.)

geometry, such as the position or shape of air holes, are used as input parameters for FDTD simulation in order to obtain the transmission spectrum. In this subsection, the sensing effects are evaluated for two different cases: longitudinal pressure (Fy) and transverse pressure (Fx). The pressure F is applied on the free boundaries of the PhC structure and the induced variation for different geometries will be calculated according to Young's module. The material is assumed to be isotropic, linear, and elastic. The structural responses are calculated by solving material elasticity matrix according to Hoke's Law under Mindlin assumption [22]. Moreover, the density (ρ), Young's module (Y_0), and Poisson ratio (σ) of silicon are 2330 kg/m^3, 1.31×10^{11} Pa, and 0.27, respectively. The deformation of PhC structure under different applied pressure is all solved every substep. By using FEM, we simulate the structural variation under the applied pressure, where the pressures considered are 0.1 μN, −0.1 μN, 0.2 μN, −0.2 μN, 0.3 μN, −0.3 μN, 0.4 μN, and −0.4 μN (The F means compression and the $-F$ means tension). This clearly shows that air holes are distorted and relocated. The new positions and shapes of the air holes are calculated as shown in schematically in Fig. 4. Fig. 4(a) and (b) shows the deformed PhC structure contour plot of displacement vector sum with the pressure of −0.4 μN in two directions, respectively. In the end, the changes of position and shape of air holes are used as the input parameters in FDTD simulation.

3.2. Structural variation in upright direction

The inserted rod is located on the modified center-defect microcavity and attached to a Si-strip which can be deformed by applied pressure. Due to the pressure displacement of Si-strip, the depth of inserted rod in the modified center-defect microcavity will be changed, as demonstrated in Ref. [1]. Yang et al. [1] showed that the structural variation Δh (the insert depth change of rod) was dependent on the mechanical properties of the top Si-strip when the applied pressure F was on the Si-strip. In this subsection, the sensing effects are evaluated for the upright direction.

Fig. 5(a) shows the schematic for the top Si-strip. The Si-strip membrane is with length and width of $l_{strip} = 50$ μm and $w = 10$ μm, respectively. In FEM simulations, the calculated Si-strip membrane is divided into

Please cite this article in press as: J. Zhou, et al. Multi-directional ultra-high sensitive pressure sensor based on the integration of optimized double 60° bend waveguides and modified center-defect photonic crystal microcavity, Photon Nanostruct: Fundam Appl (2015), http://dx.doi.org/10.1016/j.photonics.2015.01.005

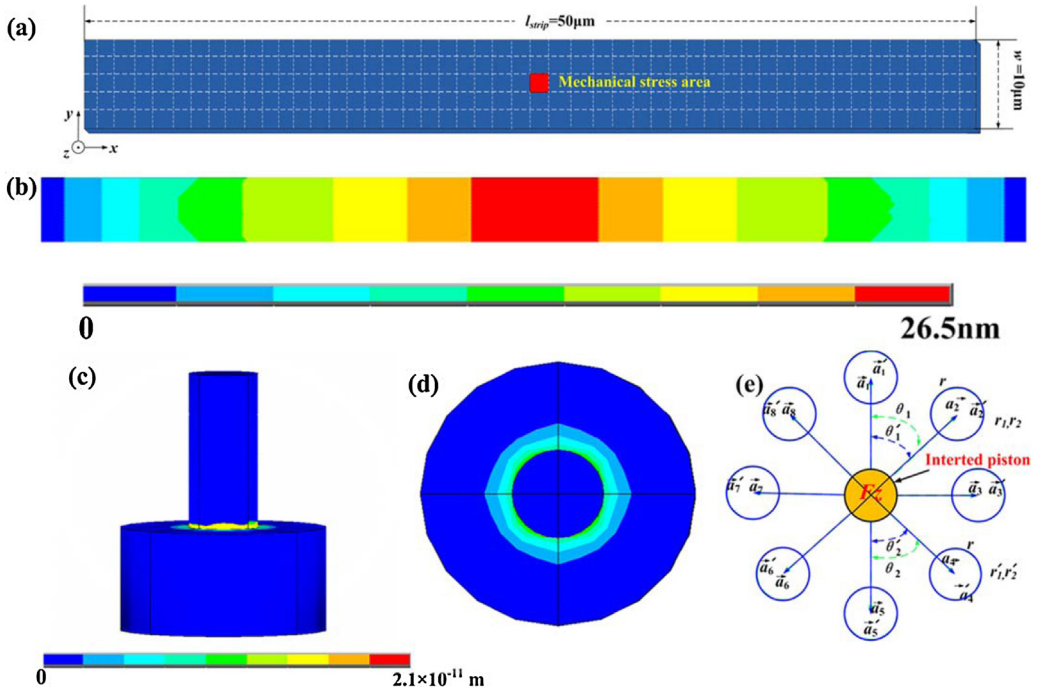

Fig. 5. (a) Schematic illustration of the top Si-strip membrane in FEM simulation. (b) The simulated pressure displacement distribution of the top Si-strip membrane when the applied pressure $F = 50$ nN. (c) The simulated PhC lattice displacement distribution of the inserted rod into the modified center-defect microcavity. (d) The simulated PhC lattice displacement distribution in x–y plane. (e) Schematic of the PhC lattice geometry changes. (For interpretation of the references to color in text, the reader is referred to the web version of this article.)

5×50 units and each unit area is $2\,\mu m^2$, where the applied pressure F is applied on the center of top Si-strip membrane (the red unit, mechanical stress area). The Si-strip membrane properties and structural response calculated method have been proposed in Section 4.1. By applying FEM simulation, the Si-strip membrane structural variation (Δh) when the applied pressure $F = 50$ nN is shown in Fig. 5(b). Fig. 6(c) presents that the deformed PhC structure contour plot of displacement vector sum when the inserted rod into the modified center-defect microcavity under the condition of applied pressure $F = 50$ nN. From Fig. 5(c)–(e), when the rod is inserted into the central hole by the applied pressure on the top Si-strip membrane, the structure around the central nanohole is only slightly influenced. Therefore, the approach of point applying pressure and the overlap of stress-applying and stress-sensing regions will not limit the flexibility in realistic situations. In addition, the torsion causing deviation from the lattice structure has been eliminated. Therefore, the proposed microcavity in the upright direction is torsion-free, relatively stable, and can be used to large pressure sensing range applications.

From the above FEM simulation results, we obtain the relationship between the applied pressure F and the structural variation Δh, as shown in Fig. 6. The calculated structural variation rate S_{h-F} of the top Si-strip membrane is 0.51 nm/nN. Due to the longer length of top Si-strip membrane, larger structural variation than that in [25] is obtained under the same applied pressure F.

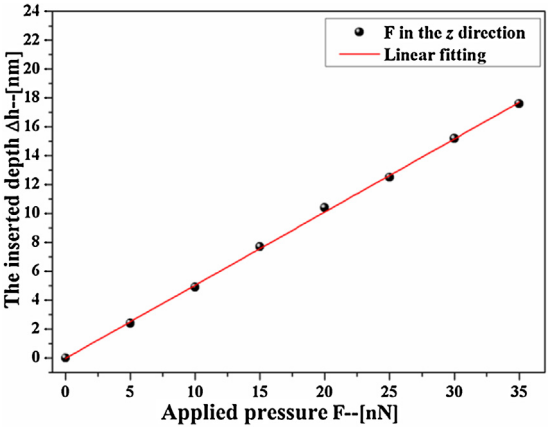

Fig. 6. The simulated relationship between the applied pressure and structural variation (Δh). The red solid-line is the linear regression result. (For interpretation of the references to color in this figure legend, the reader is referred to the web version of this article.)

Please cite this article in press as: J. Zhou, et al. Multi-directional ultra-high sensitive pressure sensor based on the integration of optimized double 60° bend waveguides and modified center-defect photonic crystal microcavity, Photon Nanostruct: Fundam Appl (2015), http://dx.doi.org/10.1016/j.photonics.2015.01.005

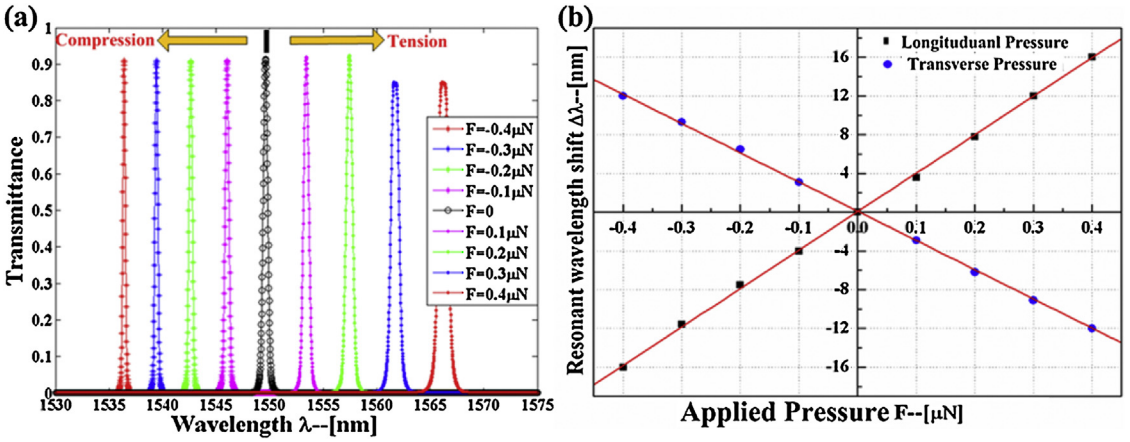

Fig. 7. (a) Transmittance spectra showing the shift the resonant wavelength under different applied pressure in longitudinal direction. (b) Resonant wavelength shift corresponding to the change in applied pressure in double directions. (For interpretation of the references to color in text, the reader is referred to the web version of this article.)

4. FDTD simulations and sensing characteristic discussion

4.1. Result and discussion in longitudinal and transverse directions

Through the design and discussion in Section 4.1, we demonstrate and analyze the performance (sensitivity and resolution) by FDTD simulation. Both tension and compression are considered in Fig. 7. Fig. 7(a) shows the shift in the resonant wavelength results from the longitudinal pressure. Under longitudinal tensile pressure, the resonant wavelength tends to shift to a longer wavelength (red shift), whereas it tends toward a shorter wavelength (blue shift) under transverse tensile pressure. We also find the intensity of the wavelength peak is pushed down a litter when the longitudinal compressive pressure or transverse tensile pressure becomes larger. This decay is mainly caused by the bigger shape and change of air holes around the microcavity. In addition, the reduction of intensity is related to the variation of coupling waveguides. With the results from FEM and FDTD simulations plugging into the expression in [22], the wavelength shifts are calculated to be 39.7 nm/μN and 30.2 nm/μN for longitudinal and transverse pressure, respectively. Furthermore, with the calculated expression in [25], the minimum detectable pressure variation δF obtained is 1.08 nN and 1.43 nN in the longitudinal and transverse direction. Compared with the ring-resonator based pressure sensor demonstrated by Zhao et al. [41], where the pressure sensitivity was only 0.65 nm/μN, the sensitivity presented in this work is largely enhanced. Meanwhile, in contrast with the L3-type resonator cavity based pressure sensor demonstrated by Yang et al. [20], where the minimum detectable pressure variation was 44 nN, the minimum

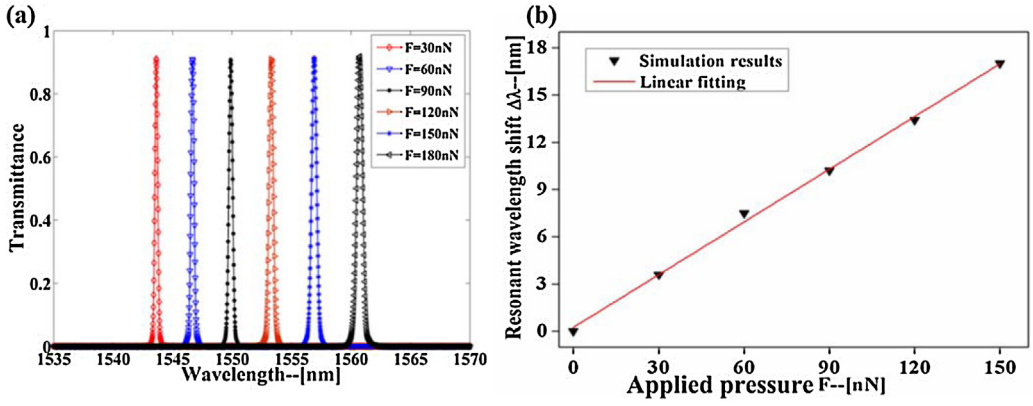

Fig. 8. (a) Simulation of transmission spectra of PhC pressure sensor under different applied pressure. (b) Resonant wavelength shift as a function of the change in applied pressure. (For interpretation of the references to color in text, the reader is referred to the web version of this article.)

Please cite this article in press as: J. Zhou, et al. Multi-directional ultra-high sensitive pressure sensor based on the integration of optimized double 60° bend waveguides and modified center-defect photonic crystal microcavity, Photon Nanostruct: Fundam Appl (2015), http://dx.doi.org/10.1016/j.photonics.2015.01.005

detectable pressure variation realized in this work is sharply reduced. The relationship between the applied pressure and resonant shift is linear in the applied pressure range. The linear relationship predicts that it is feasible way to sensing pressure with this micaocavity structure. Fig. 7(b) shows the simulation results for the shift in the resonant wavelength due to the applied pressure in the longitudinal and transverse direction. The shifts in double directions are at the same level indicating that this designed microcavity can reduce the anisotropic property of traditional pressure sensors.

4.2. Result and discussion in upright direction

Based on the design and the discussion of the dependence of PhC modified center-defect on the inserted rod and mechanical characteristic in Section 4.2, the upright directional pressure sensor design and performance will be investigated in this section. By applying the FDTD simulation and FEM method, we calculate the transmittance spectra for different values of the applied pressure. As seen from Fig. 8(a), the resonant wavelength peak tends toward a longer wavelength (red shift) when the applied pressure increases. As expected, the insert depth of rod is increased as the applied pressure improves. Accordingly, the cavity resonant wavelength is pushed toward to longer wavelength because of the increase in high-dielectric material in the cavity region. As seen in Fig. 8(b), the resonant wavelength shift is linearly proportional to the applied pressure. Thus, the sensitivity of pressure sensor is equal to 0.12 nm/nN. In addition, the calculated minimum detectable pressure variation is 0.36 nN. Compared with the side-coupled piston-type microcavity based pressure sensor investigated by Yang et al. [25], though where the pressure sensitivity is superior to that in this work, the minimum detectable pressure variation is reduced by two-fold.

5. Conclusions

In this work, a nanoscale photonic crystal pressure sensor based on the integration of optimized double 60° bend waveguides and modified center-defect microcavity is demonstrated. The applied pressure can be measured via the output transmission spectrum shift. Highly sensitive pressure sensing performance in three directions has been investigated. The pressure-induced optical properties of PhC microcavity are theoretically studied by using the combination of FEM and FDTD simulations. The results highlight a linear relationship between the applied pressure and the shift in the resonant wavelength. The high sensitivities of 39.70 nm/μN in longitudinal direction, 30.20 nm/μN in transverse direction and 0.12 nm/nN in upright direction are obtained, respectively. The low minimum detectable pressure is estimated to be as small as 1.08 nN, 1.43 nN and 0.36 nN in longitudinal, transverse and upright direction, respectively. The initially obtained results from this study call for further research to apply this proposed PhC microcavity structure to large-scale multi-directional pressure sensor array integration.

Acknowledgements

This research was supported by National Nature Science Foundation of China (no. 61372038), National 973 Program (no. 2012CB315705), National 863 Program (no. 2011AA010305), Postgraduate Innovation Fund of SICE, BUPT, 2013 and Fund of State Key Laboratory of Information Photonics and Optical Communications (Beijing University of Posts and Telecommunications), PR China.

References

[1] Y. Yang, H. Tian, D. Yang, N. Wu, J. Zhou, Q. Liu, Y. Ji, Nanomechanical three dimensional force photonic crystal sensor using shoulder-coupled resonant cavity with an inserted pillar, Sens. Actuators A: Phys. 209 (2014) 33–40.
[2] O. Painter, R.K. Lee, A. Scherer, A. Yariv, J.D. O'Brien, P.D. Dapkus, I.I. Kim, Two-dimensional photonic band-gap defect mode laser, Science 284 (1999) 1819–1821.
[3] M. Notomi, E. Kuramochi, H. Taniyama, Ultrahigh-Q nanocavity with 1D photonic gap, Opt. Express 16 (2008) 11095–11102.
[4] H. Hagino, Y. Takahashi, Y. Tanaka, T. Asano, S. Noda, Effects of fluctuation in air hole radii and positions on optical characteristics in photonic crystal heterostructure nanocavities, Phys. Rev. B 79 (2009) 085112.
[5] T. Yoshie, A. Scherer, J. Hendrickson, G. Khitrova, H.M. Gibbs, G. Rupper, C. Ell, O.B. Shchekin, D.G. Deppe, Vacuum Rabi splitting with a single quantum dot in a photonic crystal nanocavity, Nature 432 (2004) 200–203.
[6] J. Chan, M. Eichenfield, R. Camacho, O. Painter, Optical and mechanical design of a zipper photonic crystal optomechanical cavity, Opt. Express 17 (2009) 3802–3817.
[7] M. Eichenfield, R. Camacho, J. Chan, K.J. Vahala, O. Painter, A picogram- and nanometre-scale photonic crystal optomechanical cavity, Nature 459 (2009) 550–555.
[8] S. Pal, E. Guillermain, R. Sriram, B.L. Miller, P.M. Fauchet, Silicon photonic crystal nanocavity-coupled waveguides for error-corrected optical biosensing, Biosens. Bioelectron. 26 (2011) 4024–4031.
[9] F. Hsiao, C. Lee, Computational study of photonic crystals nano-ring resonator for biochemical sensing, IEEE Sens. J. 10 (2010) 1185–1191.
[10] J.O. Grepstad, P. Kaspar, O. Solgaard, I. Johansen, A.S. Sudbø, Photonic crystal membranes for optical detection of single nanoparticles, designed for biosensor application, Opt. Express 20 (2012) 7954–7965.

Please cite this article in press as: J. Zhou, et al. Multi-directional ultra-high sensitive pressure sensor based on the integration of optimized double 60° bend waveguides and modified center-defect photonic crystal microcavity, Photon Nanostruct: Fundam Appl (2015), http://dx.doi.org/10.1016/j.photonics.2015.01.005

[11] W. Lai, S. Chakravarty, Y. Zou, R. Chen, Silicon nano-membrane based photonic crystal micro cavities for high sensitivity bio-sensing, Opt. Lett. 37 (2012) 1208–1210.
[12] B. Wang, T. Siahaan, M. Dündar, R. Nötzel, M. Hoek, S. He, R. Heijden, Photonic crystal cavity on optical fiber facet for refractive index sensing, Opt. Lett. 37 (2012) 833–835.
[13] S. Kalchmair, R. Gansch, S.I. Ahn, A.M. Andrews, H. Detz, T. Zederbauer, E. Mujagić, P. Reininger, G. Lasser, W. Schrenk, G. Strasser, Detectivity enhancement in quantum well infrared photodetectors utilizing a photonic crystal slab resonator, Opt. Express 20 (2012) 5622–5628.
[14] S. Mandal, D. Erickson, Nanoscale optofluidic sensor arrays, Opt. Express 16 (2008) 1623–1631.
[15] D. Yang, H. Tian, Y. Ji, Nanoscale photonic crystal sensor arrays on monolithic substrates using side-coupled resonant cavity arrays, Opt. Express 19 (2011) 20023–20034.
[16] Z. Xu, L. Cao, C. Gu, Q. He, G. Jin, Micro displacement sensor based on line-defect resonant cavity in photonic crystal, Opt. Express 14 (2006) 298–305.
[17] D. Yang, H. Tian, Y. Ji, Microdisplacement sensor based on high-Q nanocavity in slot photonic crystal, Opt. Eng. 50 (2011) 054402.
[18] C. Lee, J. Thillaigovindan, Optical nanomechanical sensor using a silicon photonic crystal cantilever embedded with a nanocavity resonator, Appl. Opt. 48 (2009) 1797–1803.
[19] T.T. Mai, F. Hsiao, C. Lee, W. Xiang, C. Chen, W. Choi, Optimization and comparison of photonic crystal resonators for silicon microcantilever sensors, Sens. Actuators A: Phys. 165 (2011) 16–25.
[20] Y. Yang, D. Yang, H. Tian, Y. Ji, Photonic crystal stress sensor with high sensitivity in double directions based on shoulder-coupled aslant nanocavity, Sens. Actuators A: Phys. 193 (2013) 149–154.
[21] T. Stomeo, M. Grande, A. Qualtieri, A. Passaseo, A. Salhi, M. De Vittorio, D. Biallo, A. D'orazio, M. De Sario, V. Marrocco, V. Petruzzelli, F. Prudenzano, Fabrication of force sensors based on two-dimensional photonic crystal technology, Microelectron. Eng. 84 (2007) 1450–1453.
[22] T.W. Lu, P.T. Lee, Ultra-high sensitivity optical stress sensor based on double-layered photonic crystal microcavity, Opt. Express 17 (2009) 1518–1526.
[23] B. Tung, D. Dao, T. Ikeda, Y. Kanamori, K. Hane, S. Sugiyama, Investigation of strain sensing effect in modified single-defect photonic crystal nanocavity, Opt. Express 19 (2011) 8821–8829.
[24] M. Winger, T.D. Blasius, T.P.M. Alegre, A.H. Safavi-Naeini, S. Meenehan, J. Cohen, S. Stobbe, O. Painter, A chip-scale integrated cavity-electro-optomechanics platform, Opt. Express 19 (2011) 24905–24921.
[25] D. Yang, H. Tian, N. Wu, Y. Yang, Y. Ji, Nanoscale torsion-free photonic crystal pressure sensor with ultra-high sensitivity based on side-coupled piston-type microcavity, Sens. Actuators A: Phys. 199 (2013) 30–36.
[26] G.-H. Kim, Y.-H. Lee, Coupling of small, low-loss hexapole mode with photonic crystal slab waveguide mode, Opt. Express 12 (2004) 6624–6631.
[30] Y. Yang, H. Tian, D. Yang, N. Wu, Q. Liu, J. Zhou, K. Xun, Y. Ji, Three dimensional multifunctional nanomechanical photonic crystal sensor with high sensitivity by using pillar-inserted aslant nanocavity resonator, in: 12th International IEEE Conference on Optical Communications and Networks (ICOCN), 2013, pp. 1–4.
[31] A. Benmerkhi, M. Bouchemat, T. Bouchemat, N. Paraire, Numerical optimization of high-Q-factor photonic crystal microcavities with a graded air lattice, J. Opt. Soc. Am. B 20 (2011) 336–341.
[34] J.D. Joannopoulos, S.G. Johnson, J.N. Winn, R.D. Meade, Photonic Crystals Molding the Flow of Light, second ed., Princeton University Press, 2008.
[35] A.F. Oskooi, D. Roundy, M. Ibanescu, P. Bermel, J.D. Joannopoulos, S.G. Johnson, Meep – a flexible free-software package for electromagnetic simulations by the FDTD method, Comput. Phys. Commun. 181 (2010) 687–702.
[36] W. Zheng, M. Xing, G. Ren, S.G. Johnson, W. Zhou, W. Chen, L. Chen, Integration of a photonic crystal polarization beam splitter and waveguide bend, Opt. Express 17 (2009) 8657–8668.
[37] G. Ren, W.H. Zheng, Y.J. Zhang, K. Wang, X.Y. Du, M.X. Xing, L.H. Chen, Mode analysis and design of a low-loss photonic crystal 60° waveguide bend, J. Lightwave Technol. 26 (2008) 2215–2218.
[38] M. Askari, B. Momeni, M. Soltani, A. Adibi, Systematic design of wide-bandwidth photonic crystal waveguide bends with high transmission and low dispersion, J. Lightwave Technol. 28 (2010) 1707–1713.
[39] J. Zhou, H. Tian, D. Yang, Y. Liu, Q. Liu, Y. Ji, Ultra-broadband and ultra-low-loss photonic crystal with band-flatness waveguide 60° bend obtained based on lattice-shifted optimization, Opt. Commun. 322 (2014) 227–233.
[40] J.H. Chen, Y.T. Huang, Y.L. Yang, M.F. Lu, Design, fabrication, and characterization of Si-based ARROW-B photonic crystal sharp-bend waveguides and power splitters, J. Lightwave Technol. 30 (2012) 2345–2351.
[41] X. Zhao, J.M. Tsai, H. Cai, X.M. Ji, J. Zhou, M.H. Bao, Y.P. Huang, D.L. Kwong, A.Q. Liu, A nano-opto-mechanical pressure sensor via ring resonator, Opt. Express 20 (2012) 8535–8542.

Please cite this article in press as: J. Zhou, et al. Multi-directional ultra-high sensitive pressure sensor based on the integration of optimized double 60° bend waveguides and modified center-defect photonic crystal microcavity, Photon Nanostruct: Fundam Appl (2015), http://dx.doi.org/10.1016/j.photonics.2015.01.005